

^3He spin filter based polarized neutron capability at the NIST Center for Neutron Research

This content has been downloaded from IOPscience. Please scroll down to see the full text.

2014 J. Phys.: Conf. Ser. 528 012014

(<http://iopscience.iop.org/1742-6596/528/1/012014>)

View [the table of contents for this issue](#), or go to the [journal homepage](#) for more

Download details:

IP Address: 129.6.122.43

This content was downloaded on 28/07/2014 at 13:39

Please note that [terms and conditions apply](#).

^3He spin filter based polarized neutron capability at the NIST Center for Neutron Research

W.C. Chen^{1,2}, T.R. Gentile¹, R. Erwin¹, S. Watson¹, Q. Ye^{1,2}, K.L. Krycka¹, B.B. Maranville¹

¹ National Institute of Standards and Technology, Gaithersburg, Maryland, USA 20899

² University of Maryland, College Park, Maryland, USA 20742

E-mail: wcchen@nist.gov

Abstract.

A ^3He neutron spin filter (NSF) program for polarized neutron scattering was launched in 2006 as part of the National Institute of Standards and Technology (NIST) Center for Neutron Research (NCNR) Expansion Initiative. The goal of the project was to enhance the NCNR polarized neutron measurement capabilities. Benefitting from more than a decade's development of spin-exchange optical pumping (SEOP) at NIST, we planned to employ SEOP based ^3He neutron spin filters for the polarized neutron scattering community. These ^3He NSF devices were planned for use on different classes of polarized neutron instrumentation at the NCNR, including triple-axis spectrometers (TAS), small-angle neutron scattering instruments (SANS), reflectometers, and wide-angle polarization analysis. Among them, the BT-7 thermal TAS, NG-3 SANS, and MAGIK reflectometer have already been in the user program for routine polarized beam experiments. Wide-angle polarization analysis on Multi-Axis Crystal Spectrometer (MACS) has been developed for user experiments. We describe briefly the SEOP systems dedicated for polarized beam experiments and polarizing neutron development for each instrument class. We summarize the current status and polarized neutronic performance for each instrument. We present a ^3He NSF hardware and software interface to allow for synchronization of ^3He polarization inversion (neutron spin flipping) and free-induction decay (FID) nuclear magnetic resonance (NMR) measurements with neutron data collection.

Key words: polarized neutron, SEOP, ^3He NSF

1. Introduction

Polarized neutron scattering (PNS) is a powerful tool that probes magnetic structures and morphologies, magnetization density, and magnetic excitations in a wide range of magnetic materials. In 1939, Halpern and Johnson developed the theory of magnetic neutron scattering and showed that the scattered neutron polarization \mathbf{P}_f depends on the orientation of the wave-vector transfer \mathbf{Q} with respect to the incident neutron polarization \mathbf{P}_i as given by a classical Halpern-Johnson vector, $\mathbf{P}_f = -(\hat{\mathbf{Q}} \cdot \mathbf{P}_i)\hat{\mathbf{Q}}$, where $\hat{\mathbf{Q}} = \mathbf{Q}/|\mathbf{Q}|$ is the unit vector[1]. More extensive theoretical work on PNS was developed after Halpern and Johnson[2, 3, 4]. In 1969, Moon *et al.* experimentally demonstrated unambiguous separation of magnetic scattering from nuclear scattering, and nuclear coherent scattering from spin-incoherent scattering using uni-axial polarization analysis on a triple axis spectrometer (TAS)[5]. The uni-axial polarization analysis technique was later expanded to the *xyz* polarization analysis technique for separation of nuclear, magnetic, and spin-incoherent scattering[6]. A more complicated technique, spherical



neutron polarimetry, employed the CRYOPAD device[7] to solve intricate structures especially those exhibiting mixed magnetic domains and non-collinear spin structures[8]. Polarized neutron scattering is one of the most challenging neutron instrumentation techniques due to significant intensity reduction from polarized beam production and analysis, necessity of precise spin manipulation, and complicated data reduction and analysis. Supermirror and Heusler crystals have been successfully employed to polarize the incident beam and analyze the scattered beam for decades. Recently many modern neutron instrumentation techniques call for larger beam angular divergences and wavelength bandwidths, and a larger area of detector banks in the interest of large on-sample neutron fluxes and improved detection efficiency. This has made it difficult to apply the standard neutron polarization techniques using supermirrors or Heusler crystals. ^3He neutron spin filters (NSF) can (1) polarize a broad wavelength band of neutrons effectively; (2) polarize large area and widely divergent neutron beams; and (3) efficiently flip the neutron polarization (flipping process and efficiency are wavelength-independent) by reversing the ^3He nuclear polarization using the adiabatic past passage (AFP) nuclear magnetic resonance (NMR) technique[9]. The development of ^3He NSFs has been advanced significantly during the last decade and these NSF devices have been applied or planned to be applied to many polarized neutron instrumentation techniques in most neutron facilities worldwide[10, 11, 12, 13, 14, 15].

In 2006, the National Institute of Standards and Technology (NIST) Center for Neutron Research (NCNR) launched a multi-year Expansion Initiative to increase the cold neutron measurement capabilities. A ^3He NSF program for polarized neutron scattering became part of the Expansion Initiative with the goal of enhancing polarized neutron measurement capabilities. Previously, polarized beam capabilities at the NCNR were limited to polarization analysis on the reflectometer[16], occasionally on both thermal TAS[17] and cold TAS[18], incident polarized beam production on the NG-3 small-angle neutron scattering (SANS) instrument, and neutron spin echo (NSE) instrument[19]. These existing polarized neutron instrumentation techniques utilized supermirror polarizing devices for polarizing the incident beam and analyzing the scattered beam except that Heusler crystals were used on the decommissioned BT-2 thermal TAS. The NIST Physics Laboratory already had a program in research and development of ^3He NSFs for neutron science applications using both the spin-exchange optical pumping (SEOP) and metastability-exchange optical pumping (MEOP) methods. Based on substantial progress in SEOP[10], this method was adopted for the NCNR's ^3He NSF based polarized neutron program.

This paper presents an overview of polarized neutron development at the NCNR using ^3He NSFs over last several years and is organized as follows. Sec. 2 shows the calculated polarized neutronic performance. In Sec. 3 we describe the characteristics and performance of the SEOP system. In Sec. 4, we discuss polarized beam development using ^3He NSFs on the BT-7 thermal TAS, NG-3 SANS and the Multi-Axis Crystal Spectrometer (MACS) and their performance. In Sec. 5, we discuss the development of magnetostatic cavity devices used for different instruments. We describe a user-friendly hardware and software interface allowing for synchronization of AFP-based ^3He spin inversion and FID (free induction decay) NMR measurements in Sec. 6 and we summarize the paper in Sec. 7.

2. Polarized neutronic performance of a polarized ^3He spin filter

A ^3He neutron spin filter is a transmission-based neutron-polarizing device. The neutron transmission for each spin state through a polarized ^3He cell is given by

$$T^\pm = T_E \exp[-\mathcal{O}(1 \mp P_{\text{He}})] \quad (1)$$

where T^\pm is the transmission with neutron spin parallel (+) or antiparallel (-) to the ^3He spin. T_E is the transmission of the ^3He glass cell windows. The ^3He cells are fabricated from GE-180 glass[20], which has a typical neutron transmission of 0.87 at 5 Å for a typical large spin filter cell. The wavelength dependence of the transmission of glass cell windows has been measured

to be relatively flat[21]. P_{He} is the ^3He polarization. \mathcal{O} is the opacity of the cell. Because the neutron absorption cross section increases linearly with neutron wavelength, a practical expression for the opacity is $\mathcal{O} = 0.726p\lambda l$, where p is the ^3He gas pressure in bar for a cell at a temperature of 295 K, λ is the wavelength in nm, and l is the length of the cell in cm. \mathcal{O} is a dimensionless quantity. The transmission for an unpolarized neutron beam passing through a polarized ^3He cell is then given by

$$T_{\text{n}} = T_{\text{E}}\exp(-\mathcal{O}) \cosh(\mathcal{O}P_{\text{He}}) = T_0 \cosh(\mathcal{O}P_{\text{He}}) \quad (2)$$

where T_0 is the transmission for an unpolarized neutron beam passing through an unpolarized ^3He cell ($P_{\text{He}}=0$) and is given by $T_0 = T_{\text{E}}\exp(-\mathcal{O})$. The resulting neutron polarization after passing through a polarized ^3He cell is given by

$$P_{\text{n}} = \frac{T^+ - T^-}{T^+ + T^-} = \tanh(\mathcal{O}P_{\text{He}}) = \sqrt{1 - \frac{T_0^2}{T_{\text{n}}^2}} \quad (3)$$

The flipping ratio F of either the polarizer or analyzer is given by

$$F = \frac{T^+}{T^-} = \exp(2\mathcal{O}P_{\text{He}}) \quad (4)$$

Optimization of the trade-off between P_{n} and T_{n} depends on the experiment[22]. A common figure of merit is defined as $P_{\text{n}}^2 T_{\text{n}}$ for a polarizer. Fig. 1(a) shows polarized neutronic performance (P_{n} , T_{n} , T^+ , $P_{\text{n}}^2 T_{\text{n}}$ and F) as a function of the opacity of a ^3He cell at a ^3He polarization of 80 %, a typical value that we have achieved recently. A general rule of thumb is $P_{\text{n}}=0.96$, $T_{\text{n}}=0.27$ for $\mathcal{O}=2.5$ and $P_{\text{He}}=80$ %. $P_{\text{n}}^2 T_{\text{n}}$ has a broad peak at $\mathcal{O} \cong 2$ in Fig. 1a. In general, the opacity at which $P_{\text{n}}^2 T_{\text{n}}$ is maximized, \mathcal{O}_{p} , depends on the ^3He polarization and is given by

$$\mathcal{O}_{\text{p}} = \frac{1}{P_{\text{He}}} \tanh^{-1} \left[\frac{\sqrt{8P_{\text{He}}^2 + 1} - 1}{2P_{\text{He}}} \right] = \frac{1}{2P_{\text{He}}} \ln \frac{2P_{\text{He}} - 1 + \sqrt{8P_{\text{He}}^2 + 1}}{2P_{\text{He}} + 1 - \sqrt{8P_{\text{He}}^2 + 1}} \quad (5)$$

Fig. 1(b) shows \mathcal{O}_{p} as a function of P_{He} , indicating that \mathcal{O}_{p} is insensitive to the ^3He polarization and has a value of ≈ 2 for ^3He polarizations lower than 80 %. For ^3He polarizations ≥ 80 %, as the ^3He polarization increases, the peak location shifts towards a larger \mathcal{O}_{p} value. Fig. 1(b) also shows $P_{\text{n}}^2 T_{\text{n}}$ for $\mathcal{O} = \mathcal{O}_{\text{p}}$ as a function of the ^3He polarization. In most cases, \mathcal{O} values larger than \mathcal{O}_{p} have generally been chosen in order to reach desired neutron polarizations (flipping ratios)[22].

3. NIST SEOP systems for neutron spin filter applications

For all current neutron science applications at the NCNR, we have retrofitted ^3He NSF devices to existing instruments. Space constraints make *in-situ* SEOP on the beamline challenging, therefore we have focused on offline operation in which ^3He gas is polarized in the lab and transported to the beamline. As soon as the polarized cell is installed on the beam, the ^3He polarization starts to decay exponentially with a characteristic relaxation time T_1 assuming that the external field perturbation does not change with time. One of the major tasks for offline operation of ^3He NSFs is to achieve as long a T_1 as possible on the beamline. Space constraints and/or stray magnetic fields from the instrument itself or sample environment make T_1 's of ^3He cells shorter than intrinsic T_1 's obtained with a negligible magnetic field gradient. For most of our applications, we refresh polarized ^3He cells for each NSF device on the beam daily. It is

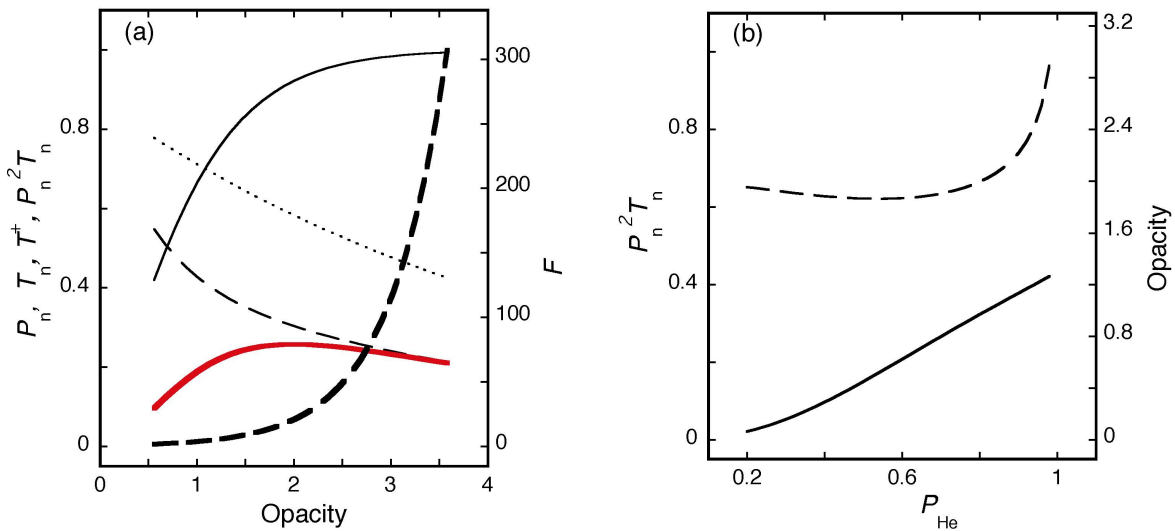


Figure 1. (Color online) (a) Neutron polarization efficiency P_n (solid thin line), transmission T_n (thin dashed line), T^+ (dotted line), a figure of merit given by $P_n^2 T_n$ (solid red thick line), and the flipping ratio F (dashed thick line) as a function of the opacity \mathcal{O} at $P_{He}=80\%$. (b) the opacity at which $P_n^2 T_n$ is maximized, \mathcal{O}_p , (dashed line) and $P_n^2 T_n$ (solid line) as a function of P_{He} . The typical empty cell transmission $T_E=0.87$ is included. Note the flipping ratio is calculated for either the polarizer or analyzer only assuming other neutron polarizing devices are perfect in efficiency as discussed in the text. All quantities in plots are dimensionless.

necessary to have multiple SEOP systems and several cells for each configuration (see the cell database in Ref. [10]). We currently have three well-characterized SEOP systems at NIST used for neutron science applications[10]. Among them, one system has been used for more than a decade for neutron spin filter research and development, and recently has been mainly employed for developing wide-angle cells[23, 24]. Two of them are dedicated to providing polarized ^3He gas for polarized neutron experiments at the NCNR[10] as shown in Fig. 2. A fourth system is planned for 2014, allowing us to provide polarized ^3He gas to more than one instrument simultaneously.

The general features of the NIST SEOP systems were described in Ref. [10]. Here we briefly describe a new feature of the three systems. Over three years ago, we implemented chirped volume holographic gratings (VHG)[26] for tunable spectral narrowing of high power laser diode bars[10]. VHGs contain planes of varying index of refraction fabricated in photorefractive glass[27, 28], that produce a wavelength-selective reflection. A chirped VHG provides a higher spectral density and better suppression of broadband background as compared to diffraction gratings[31], especially for higher power laser diodes. Recently, we switched to chirped VHGs from diffraction gratings for all high power lasers used in the three systems above. Now, each SEOP system can provide a total power up to 120 W to the optically pumped ^3He cell with a spectral linewidth (FWHM) between 0.2 nm and 0.3 nm. This change has resulted in a modest improvement in ^3He polarization. We have obtained ^3He polarizations of 80 % to 85 % on the neutron beam line for cells nearly 1 liter in volume. A detailed paper on studies of ^3He polarization improvement from use of the chirped VHGs will appear in a future publication.

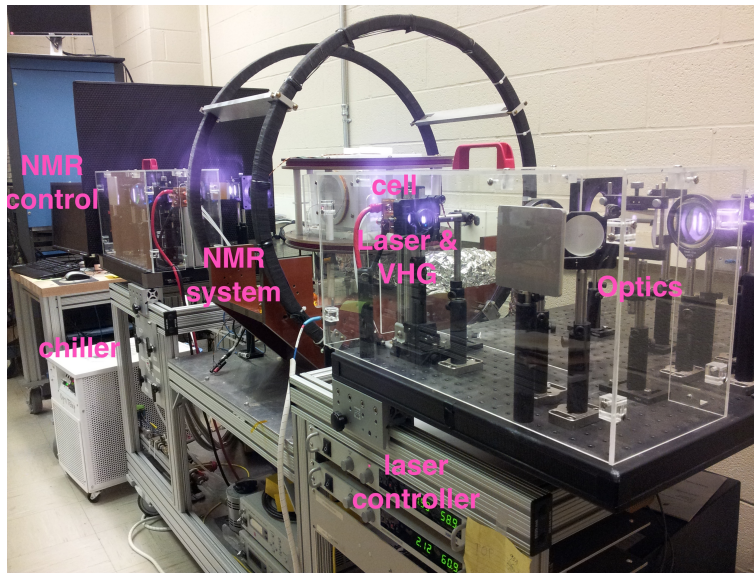


Figure 2. (Color online) One of the NIST SEOP systems showing all the components. The SEOP system includes the NMR system with three pairs of coils (holding field, radio-frequency field coils and pick-up coils) assembled orthogonally each other, NMR control system, high power diode lasers and associated controllers and chiller, and laser optics. The majority of the system is mounted to a movable aluminum 80-20[25] cart.

4. ^3He NSF applications at the NCNR

At the NCNR, we have applied ^3He NSFs to polarize incident neutrons and analyze scattered neutron beams for SANS, thermal TAS, reflectometers, an interferometer, and wide-angle polarization analysis on the Multi-Axis Crystal Spectrometer. We began providing polarized ^3He gas to user experiments in 2008. Fig. 3 summarizes usage of polarized ^3He gas for neutron science applications during the last 5 years. On average, the amount of ^3He gas polarized is about 150 bar-liter per year for both routine user experiments and ^3He NSF tests.

4.1. Polarization analysis on the BT-7 thermal triple axis spectrometer

On the BT-7 thermal TAS, incident neutrons, after passing through a 20 cm by 20 cm double-focusing monochromator of either pyrolytic-graphite(PG)(002) or copper(Cu)(220)[32], are polarized by a ^3He NSF device and the scattered neutrons are analyzed by a second ^3He NSF device[33]. The maximum beam size at both the ^3He polarizer and analyzer is 10 cm in height and 5 cm in width. The ^3He polarization of the analyzer was maintained by a magnetically shielded solenoid (MSS)[33, 34], which is attached to the detector arm and located approximately midway between the sample and the PG energy analyzer. For the polarizer, we first employed a MSS to maintain the ^3He polarization, but have recently switched to a compact “Magic Box”[35, 36] to facilitate the neutron spin transport[34]. In order to reduce the relaxation rate of the ^3He polarization induced by magnetic field gradients[37], we have developed a new magic box for which the mu-metal thickness was doubled from 1.6 mm to 3.2 mm so that it can be operated at a higher field (from 2.3 mT to 3.6 mT) without magnetically saturating the mu-metal. Note that the drive sections of the high field magic box where magnetic coils are located have a total thickness of 6.4 mm. For a typical polarized TAS setup, it is essential to have a capability of longitudinal polarization analysis in both $\mathbf{P} \perp \mathbf{Q}$ and $\mathbf{P} \parallel \mathbf{Q}$ configurations[5] at low sample fields. It is also necessary to be able to measure four spin-dependent cross sections in each

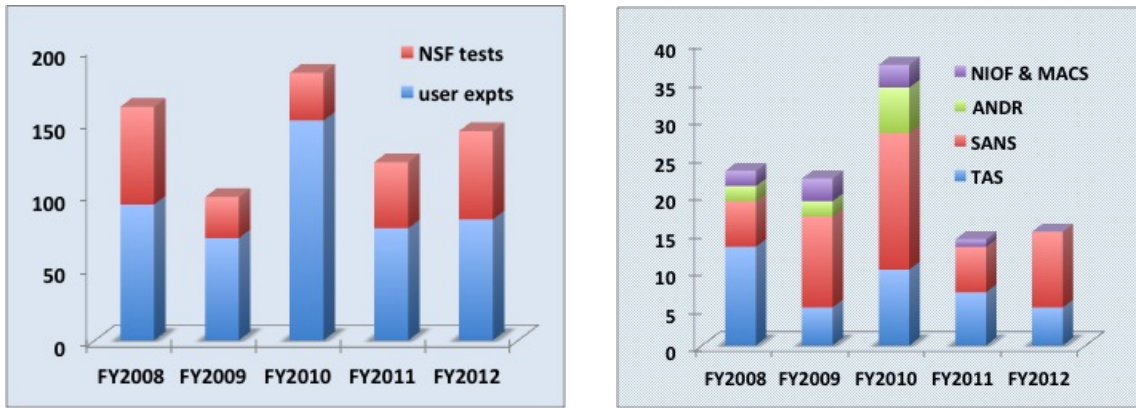


Figure 3. (Color online) Amount of polarized ³He gas produced during the last 5 years (left plot). This includes ³He gas polarized for user experiments and NSF tests. Applications of ³He NSFs to different polarized instruments at the NCNR during the last 5 years (right plot). The instruments that employed ³He NSFs were BT-7 TAS, NG-3 SANS, ANDR reflectometer, MACS, and Neutron Interferometer and Optics Facility (NIOF)[29, 30]. Note the reactor at the NCNR was down from April, 2011 to March, 2012.

configuration. The polarization flipping for both incident and scattered beams was controlled by a precession coil neutron spin flipper at the beginning of polarized beam development on BT-7 in 2006. Because we retrofitted our ³He NSF devices onto the instrument, space was limited for polarized beam implementation. Thus, the neutron spin flipper could only be situated near the sample field coils that provided the neutron polarization axes ($P \perp Q$ and $P \parallel Q$), as mentioned above. For $P \parallel Q$, two issues arose at large scattering angles: (1) decrease of the spin flipper efficiency and (2) non-adiabatic spin transport between the flipper and the sample field. Consequently, the polarized beam setup limited polarization analysis for the $P \parallel Q$ configuration to elastic diffraction experiments at small scattering angles.

Recently we re-designed the polarized beam instrumentation on the BT-7 TAS. The new setup employs newly designed, compact adiabatic spin rotation devices and nearly lossless neutron spin inversion using AFP to invert the ³He polarization[38]. The new apparatus avoids using a precession coil spin flipper and frees up an additional space of ≈ 10 cm, which is enough for adiabatic spin transport. The new polarized beam setup on the BT-7 TAS is entirely contained within the ³He NSFs (³He polarizer and analyzer) without the need for external spin flipping devices, resulting in significantly improved polarized neutronic performance. Here, we present a brief summary of the performance. The details of the design and characterization of polarized beam configuration will appear in a future paper.

There are several new notable features for the new polarized beam setup. First, polarized beam calibration is simpler and easier. Using the polarized beam setup provided by the ³He NSFs, it is easy and straightforward to obtain polarization efficiencies since the polarizing efficiencies of the polarizer and analyzer are independently measured from the neutron transmissions or calculated from the ³He polarization[39]. Previously for a conventional polarized beam setup, it was necessary to measure the four spin dependent transmissions using a sample whose spin cross sections are well known to extract polarizing efficiencies of polarizing elements (polarizer, analyzer, each flipper)[40, 41]. The second feature of the new setup is a truly adiabatic spin transport along the entire neutron path. After polarized beam calibration, we characterized the energy dependence and spatial uniformity of the spin transport efficiency. We determined that the overall spin transport efficiency is better than 99 % for neutron energies up to 50 meV

for both the $\mathbf{P} \perp \mathbf{Q}$ and $\mathbf{P} \parallel \mathbf{Q}$ configurations. We found that the spin transport efficiency is uniform for a wide range of scattering angles, a feature required for the $\mathbf{P} \parallel \mathbf{Q}$ configuration. The ^3He AFP based neutron spin flipping efficiency was nearly 100 % and energy-independent except for a tiny irrecoverable ^3He polarization loss per flip. This loss was determined to be $\approx 1 \times 10^{-5}$ and $\approx 3 \times 10^{-5}$ for the polarizer and analyzer, respectively, on BT-7. The nearly lossless ^3He polarization per flip is one of the key features as it is desirable to have the loss lower than 1×10^{-4} per flip if flipping happens within several minutes in order to avoid an additional apparent contribution to the effective T_1 . For 1×10^{-4} loss, the additional T_1 contribution is ≈ 1000 h for a flip every 0.1 h. Lastly, the ^3He polarization was improved from a previous value of 75 % to a current value of 80 % due to use of chirped VHGs described in Sec. 3.

After we fully characterized all polarizing elements, we have tested the new polarized setup to establish the level of performance. We first tested the polarized inelastic performance. This is the most demanding test because spin transport becomes more difficult at higher neutron energies. For this test, we employed the ^3He cell Grigio as a polarizer and the cell Sangiovese as an analyzer. Grigio had an opacity of 4.04 at 14.7 meV and its ^3He polarization was 80 %. Sangiovese had an opacity of 3.02 at 14.7 meV and its ^3He polarization was 78 %. Both cells are cylindrical, have a diameter of ≈ 11 cm and a volume of 0.95 liter. We obtained a flipping ratio of 85 for a fully open beam (maximum beam size) with an intensity reduction factor of only 12.0 (both polarizer and analyzer are accounted for) at a neutron energy of 14.7 meV compared to an unpolarized beam configuration; While the measured flipping ratio was reduced to 8.4 at 50 meV, the intensity reduction factor was reduced to 5.9 at 50 meV (overall transmission improved by a factor of 2). The decrease in the flipping ratio and increase in intensity at 50 meV are due to the energy-dependence of the ^3He NSF as described in Sec. 2. The calculated flipping ratios were 90 and 8.6 for 14.7 meV and 50 meV, hence the spin transport is nearly perfect at both 14.7 meV and 50 meV.

For the polarized elastic condition, we employed the cell Viognier as polarizer and Syrah as analyzer. Opacities were 3.11 and 2.29 for Viognier and Syrah both at 14.7 meV. ^3He polarizations were 80 % for both cells. We obtained a flipping ratio of 30 for a fully open beam with an intensity reduction factor of only 7.7 at a neutron energy of 14.7 meV. Based on the flux measurement[32] in unpolarized mode and a typical transmission of 0.25 for the polarizer, the polarized flux at the sample was calculated to be $0.6 \times 10^7 \text{ cm}^{-2}\text{s}^{-1}$ at 14.7 meV with the PG(002) monochromator vertically focused and $1.1 \times 10^7 \text{ cm}^{-2}\text{s}^{-1}$ at 13.7 meV with the monochromator doubly focused, both with a PG filter. Such polarized flux values are comparable to those from instruments IN20 ($1.05 \times 10^7 \text{ cm}^{-2}\text{s}^{-1}$) and IN22 ($0.75 \times 10^7 \text{ cm}^{-2}\text{s}^{-1}$) at 14.7 meV at the ILL (Institut Laue-Langevin)[42]. This showed that ^3He NSFs in combination with a PG(002) monochromator at ^3He polarizations of 80 % well outperformed Heusler crystals. Although the performance of Heusler crystals has improved during the last several years, Kulda *et al.* showed a ^3He NSF with a PG monochromator outperformed a Heusler crystal monochromator for wavelengths below 0.18 nm even with a ^3He polarization of 48 %[43]. The polarized beam capability with ^3He NSFs on the BT-7 thermal TAS at the NCNR has been applied to studies of multiferroics[44, 45, 46], superconductivity[47, 48], and magnetic thin films[49]. All these applications were done with the old polarized BT-7 setup where ^3He polarizer and analyzer and precession coil flippers were used.

4.2. Polarization analysis on the NG-3 SANS instrument

We have recently developed SANS polarization analysis on the NG-3 SANS instrument using a ^3He NSF[34, 50, 51]. Spin-analyzed SANS is a powerful probe for studies of magnetic morphology with directional sensitivity. The SANS polarization analysis technique developed at the NCNR has recently been employed for hard condensed matter investigations such as magnetic nanoparticles[52, 53, 54], an exchanged-biased system[55], multiferroics[56, 57], and

a giant magnetostrictor[58]. For a typical spin-analyzed SANS setup as shown in Fig. 4, a V-shape Fe/Si supermirror in a transmission geometry is used to polarize the incident neutrons. A precession coil spin flipper is placed immediately after the polarizer. A ^3He analyzer is used to spin-analyze the scattered beam from the sample. For the setup, the limited space and a modest stray field from the 1.6 T sample field have prevented us from operating precession coil spin flipper and radio-frequency flippers, positioned immediately after the sample. Therefore, the neutron spin flipping for the scattered beam is done by inverting the ^3He polarization using the AFP NMR technique. The ^3He polarization of the analyzer is maintained by a compact MSS. The radio-frequency coil required for the ^3He polarization inversion was provided by a $\sin\theta$ coil[38], 17 cm in diameter and 20 cm long, to provide an RF magnetic field of 0.02 mT orthogonal to the main holding field without adding material in the beam. The entire ^3He analyzer system is under vacuum to minimize air scattering.

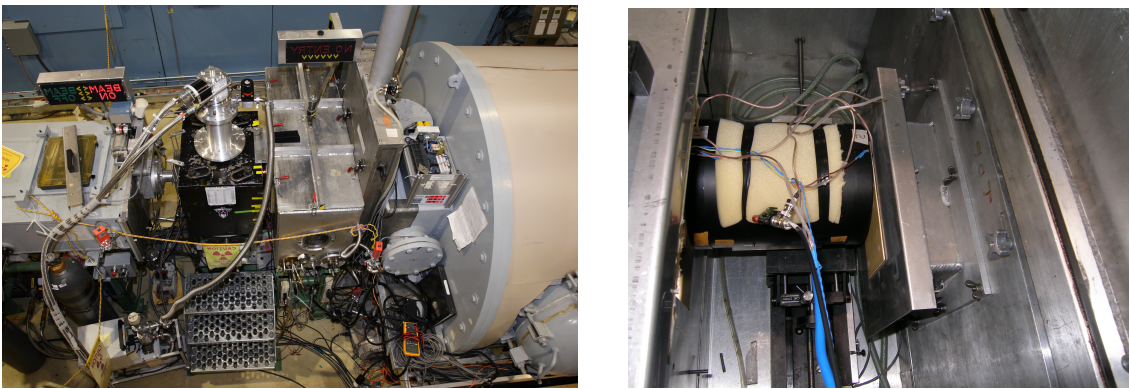


Figure 4. (Color online) A spin-analyzed SANS setup on the NG-3 SANS instrument at the NCNR (the left picture). The neutron beam travels from left to right in the pictures. In the middle of the picture is the 1.6 T electromagnet (black cubic object) with an iron-yoke field return path for reducing the stray field. A supermirror and a spin flipper are located further upstream of the magnet (not shown in the picture). A sample chamber that can be either under vacuum or in air is attached upstream of the large detector tank. Between the magnet and sample chamber, there is an 8-cm gap where an adiabatic spin rotator is located. The MSS maintaining the ^3He polarization is located inside the sample chamber and under vacuum during the experiment. The right picture shows a view of the MSS inside the chamber.

In the last few years, a few new features have been developed for improving the SANS polarization analysis capability. The most important improvement is to achieve as large a Q as possible while still maintaining reasonably long relaxation times even at a field of 1.6 T. The length scale of the magnetic features is inversely proportional to Q . For SANS polarization analysis setup combined with a high sample field (≥ 1 T), the achievable maximum Q is smaller than the instrumental Q_{max} defined in the unpolarized setup. The SANS polarization analysis setup has limited the size of magnetic nanoparticles larger than 9 nm for studies of magnetic morphologies at fields lower than saturation[52]. Even for studies of the nanocrystalline alloy at a saturating field, SANS polarization analysis has precluded detection of a magnetic peak at 17 nm[59]. Achieving a larger Q_{max} becomes an essential and challenging task when implementing SANS polarization analysis. This requires either maximizing the diameter of the analyzer cell or minimizing the distance between the sample magnet and the ^3He NSF analyzer or both. Fabricating a large diameter ^3He cell is practically difficult[10] requiring a larger magnetostatic cavity device, thus demanding more space. A decade of SEOP ^3He cell

development has led to the ability to make cells with a diameter of 12–13 cm, , currently limited by our GE-180 glass blowing technology. Therefore the most effective method is to decrease the distance between the magnet and analyzer, but this deteriorated the field gradient of the MSS due to a large stray field from the magnet, hence the relaxation time of the ^3He polarization decreased. Neutron depolarization from a field direction rotation in the region might also be an issue. During the last few years, we have developed a compact system that can reach Q_{max} of 1 nm^{-1} or higher without offsetting the analyzer cell, while providing the adiabatic spin transport for the overall large, divergent scattered beam and maintaining the relaxation time $\geq 100 \text{ h}$.

Here we present a brief summary of the system. The electromagnet we have used provides a field to the sample up to 1.6 T with the field direction with the field direction perpendicular to the beam in the horizontal plane. The magnet was specifically modified with a proper iron-yoke to minimize the stray field at the ^3He analyzer. The yoke is 23 cm from the center of the magnet to the edge and the stray field was about 2.5 mT at a position of 8 cm away from the edge of the magnet where the MSS is located. For a MSS, a large hole in each end cap at both ends is necessary for the neutron path. As the hole becomes larger, Q_{max} becomes larger if the cell diameter is not a limiting factor, but the field leakage to the inside solenoid is higher and the field gradient at the polarized ^3He cell is worse. Consequently the T_1 of the ^3He analyzer cell is shorter. We have developed MSSs of different sizes for a trade-off between Q_{max} and relaxation times as described in Table 1 in Sec. 5. Furthermore, the 8 cm gap between the MSS and magnet required that an adequate, compact spin rotation device be developed to ensure the neutron spin for the entire scattered beam is adiabatically rotated from the transverse horizontal to longitudinal direction within a short distance. We measured four spin-dependent transmissions on the main beam to perform the polarized beam calibration[50, 51] and determined the spin transport was $\geq 99\%$. Mapping the overall instrumental polarization efficiency pixel by pixel on the two-dimensional PSD (position sensitive detector)[60] provided an additional check of the spin transport efficiency for all scattered beams. Using this method, we determined that the spin transport for the entire beam path in our polarized beam setup was $\geq 99\%$. Finally, the ^3He polarization loss was determined to be better than 1×10^{-4} per flip even when the magnet operates at 1.6 T. Given a typical polarized SANS measurement time of half an hour, the loss induced a negligible difference in T_1 compared to no ^3He flipping.

We routinely operate the polarized SANS setup at two wavelengths, 5 Å and 7.5 Å. We obtained an instrumental flipping ratio of typically 13 at 5 Å and 19 at 7.5 Å if there is no sample depolarization. The instrumental flipping ratio F is given by $F = \frac{(1+P)}{(1-P)}$, where P is the instrumental polarization efficiency. These low flipping ratios are mainly limited by the supermirror polarizer and the spin flipper on the NG-3 SANS instrument. The polarizing efficiency of the single V-shaped Fe/Si supermirror is wavelength dependent, 0.89 and 0.94 for 5 Å and 7.5 Å, respectively. The flipper efficiency is 0.97 (0.985 flipping probability) for both wavelengths. The supermirror polarizer and spin flipper together limit the flipping ratio to be 14 at 5 Å and 21 at 7.5 Å. More recently, we relocated polarized beam experiments from the NG-3 SANS to the NG-7 SANS instrument. At the same time, the NCNR installed a double V-shaped supermirror and an RF flipper for the incident beam to improve the spin flipping efficiency. The new supermirror is expected to have much better polarization efficiency (95 % at 5 Å and 99 % at 7.5 Å). The RF flipper is wavelength-independent and expected to be insensitive to the large wavelength spread present in SANS ($\geq 11\%$). It is anticipated to have a flipping efficiency better than 99 %. In these new configurations, the flipping ratios are estimated to be higher than 27 and 55 for 5 Å and 7.5 Å, depending on the final performance of the new supermirror and RF flipper. The transmission of the current polarizer was measured to be 36 %, which for a typical ^3He analyzer cell yields an initial intensity loss factor of 5.5 compared to an unpolarized beam.

Another important development was to characterize the spatial variations in polarized neutronic performance[60]. For most of our applications using ^3He NSF's, the ends of the

blown cylindrical ^3He cells are often made rounded for better structural integrity, so the ^3He gas thickness may differ for different scattered beams. We have characterized the two-dimensional neutron path variations in opacity, transmission through polarized ^3He cells, and neutron polarization generated from a ^3He NSF. We found the path length variations in opacity and transmission are about 10 % and 8 %, respectively, from the cell center to the edge for a typical SANS polarization analysis configuration. However, the overall instrumental polarization efficiency is spatially uniform and its variation is about 1 % [60]. Although the spatial variations are not large, it should be corrected for when performing polarization efficiency corrections.

4.3. Wide-angle polarization analysis

Our apparatus for wide-angle neutron polarization analysis [23] consists of a vertical, neutron-compatible, solenoid that contains spin filter polarizer and analyzer cells close to the tail of a sample cryostat. The polarizer cell is contained in a shielded RF solenoid to permit inversion of the ^3He polarization via AFP without loss of polarization in the analyzer cell. The wide-angle cells cover an angular range of up to 110° on either side of the neutron beam. FID is used to monitor the ^3He polarization in the spin filter cells. Using conventional cylindrical cells [10], the apparatus was employed for a study of superconducting $\text{Fe}_{1+y}\text{Te}_{0.62}\text{Se}_{0.38}$ [61] on MACS [62]. Recently we reported several upgrades to this apparatus [24], in particular the development of GE180 [20] wide-angle cells with relaxation times between 100 h and 400 h, and ^3He polarization values, P_{He} , between 0.65 and 0.80. A new measurement in the largest wide-angle cell (denoted Giant, volume of 1.3 liters) yielded $P_{\text{He}}=0.77$ and a relaxation time of 400 h. For this test, the cells were pumped by two 100 W single-bar diode lasers narrowed with chirped VHGs as described in Sec. 3 and an additional 50 W spectrally narrowed laser [63] supplemented the illumination on the ends of the cell.

In April 2013 the upgraded apparatus was tested on MACS (see Fig. 5). Although the MACS apparatus is nominally non-magnetic, we discovered a stray magnetic field from the MACS pre-sample optics that reduced the ^3He relaxation times. A mu-metal shield located between the optics and the spin filter apparatus effectively blocked the stray field and improved the field homogeneity at the cells. For the polarizer cell Mourvedre, we obtained a relaxation time $T_1=156$ h (340 h off-line) and for the analyzer cell Giant we obtained 240 h (400 h off-line). With an improved AFP scheme, the loss per flip for the polarizer was 0.10 % per flip and the associated loss in the analyzer cell was 0.005 % per flip. Four polarizer cells with typical relaxation times of 200 h and opacity values between 2.2 and 4.8 at 5 \AA have been fabricated. The apparatus will be further tested on MACS in Oct. 2013, and we expect to conduct a neutron scattering experiment soon thereafter.

5. Development of magnetostatic cavity devices

The magnetic field gradient ($|\vec{\nabla} B_{\perp}/B|$) induced ^3He polarization relaxation rate is proportional to the square of the gradient and inversely proportional to the partial ^3He pressure [37]. On the beam line, the space is often limited for implementation of ^3He NSFs. However it is still desired to have a field gradient of $5 \times 10^{-4} \text{ cm}^{-1}$ or better so that the field gradient contribution to the relaxation time of the ^3He polarization is 600 h or longer at a ^3He pressure of 1 bar. For cells used on the beam line, the relaxation times are typically 300 h in a pair of large Helmholtz coils. The relaxation times would reduce to 200 h at a ^3He pressure of 1 bar under such a field gradient on the beam line. In addition, when designing magnetostatic cavities it is necessary to connect their magnetic field to the neighboring fields for adiabatic neutron spin transport. Neutron depolarization can occur if a neutron traverses a region in which the magnetic field direction rotates faster than its Larmor precession frequency. Hence, it is necessary to either avoid spin rotation or obtain adiabatic spin transport when designing magnetostatic cavity devices.

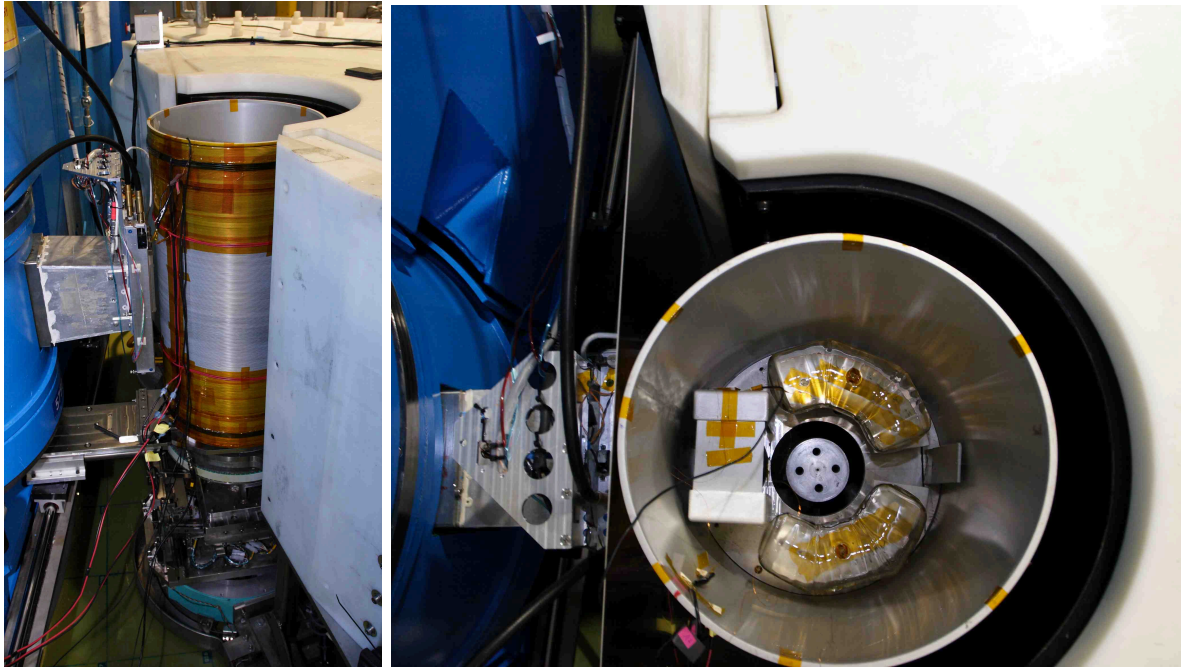


Figure 5. (Color online) Photographs of the spin filter apparatus on MACS during the April 2013 test run, without the sample cryostat. The neutron beam exits the monochromator drum (blue, left), passes through the MACS pre-sample optics and into the vertical solenoid. Inside the solenoid (right photo), the beam passes through the metal box containing the polarizer cell and scattered neutrons pass through the analyzer cells. The mu-metal shield discussed in the text can be seen between the pre-sample optics and the solenoid.

Over the last decade, we have developed two types of magnetostatic cavity devices that can provide a large volume, uniform magnetic field for different polarized beam instruments at the NCNR: magnetically shielded solenoids[22, 33, 34, 64, 65] and end-compensated magic boxes[34, 36]. A MSS consists of a solenoid with a cylindrical mu-metal shielding co-axial with the solenoid. Two mu-metal end caps with a hole to pass neutrons are snugly attached to each end of the cylindrical magnetic shielding. Typically our single-layer MSS can tolerate an external stray field up to 2.5 mT and still provide a reasonable field gradient for the ^3He cell contained inside for user experiments. A MSS provides a field along the neutron beam line, which often requires an adiabatic $\pi/2$ rotation of neutron spins. Table 1 lists MSSs used on different instruments at the NCNR. For the most compact MSS called Kronos, the field gradient on the NG-3 SANS instrument resulted in a T_1 decrease from 150 h to between 50 h and 90 h, but it yielded a Q increase $\approx 40\%$ higher compared to MSSs called Gemini and Pollux. Both Gemini and Pollux MSS can have T_1 's longer than 200 h. To provide a longer T_1 than the MSS Kronos, but maintain the same Q , we developed a double layer MSS called Artemis. The outer shielding is made of lower permeability NETIC[66] mu-metal nested around an inner high permeability CO-NETIC[66] mu-metal shield. The compensation coils are attached to the inner end-caps. We obtained a T_1 of 150 h even with the sample magnet operating at 1.6 T for the MSS Artemis, indicating that the field gradient induced relaxation time is a factor of ≈ 4 , after correction to the cell T_1 of 400 h in a non-gradient limited field such as a pair of large Helmholtz coils, longer than that in the MSS Kronos, without decreasing the achievable Q_{max} .

A magic box is a coil driven magnetic parallel plate capacitor made of high permeability

CO-NETIC[66] mu-metal. An end-compensated magic box has a short magic box (hence compensated) attached to each end of the box with a small air gap between each section[36]. This minimizes end-effects from a finite magic box and improves the field gradient for a compact box with dimensional constraints. We have demonstrated that the gradient-induced relaxation rate of the ^3He polarization for an end-compensated box can be an order of magnitude smaller than that of an uncompensated box[36]. However, experience has shown the box is sensitive to external field gradients, especially a gradient component orthogonal to the holding field[34]. As described in Sec. 4.1, an effective way to minimize the gradient-induced relaxation is to increase the holding field, but without saturating the mu-metal. We constructed a high field magic box made of two layers of mu-metal in the top and bottom magnetic connecting plates and four layers of mu-metal in the drive sections for both the main section and two compensating sections. Table 2 lists two boxes we constructed, one with a single-layer and the other with a double layer, and their performance in the lab and on the beam line. Note that the normalized field gradient on the beam line is sensitive to the external stray field magnitude, and we show the range of the gradient when possible. The lower value corresponds to a stray field of less than 0.1 mT and the higher value corresponds to a stray field of about 0.3 mT. As the holding field of the double-layer box Flattop was increased, the normalized volume-averaged gradient decreased. Increasing the field from 0.9 mT to 3.6 mT improved the relaxation time by more than an order of magnitude.

Table 1. Magnetically shielded solenoids used on different neutron beamlines at the NCNR. D is the outside diameter in cm of the mu-metal shielding, l is the outside length in cm of the shielding, and d_{ec} is the diameter of the end cap hole to pass neutrons. $|\vec{\nabla}B_{\perp}/B|^i$ is the volume-averaged field gradient determined from T_1 's measured without any stray field for a cylindrical cell 12 cm in diameter and 8 cm long. $|\vec{\nabla}B_{\perp}/B|^b$ is the volume-averaged gradient determined from T_1 's measured often with modest stray fields from the sample field and/or adiabatic spin rotation devices on the beam line. On the NG-3 SANS instrument, the stray field is dominated by the 1.6 T electromagnet located very close to the MSS to maintain the ^3He polarization of the analyzer. The MSS Artemis has two layers of nested magnetic shielding. The outer shielding is NETIC [66] mu-metal and the inner shielding is CO-NETIC[66] mu-metal. The compensation coils are attached to the inner end-caps. The first (second) number in D , l and d_{ec} refer to parameters for the inner (outer) layer shielding.

MSS name	D cm	l cm	d_{ec} cm	$ \vec{\nabla}B_{\perp}/B ^i$ 10^{-4} cm^{-1}	$ \vec{\nabla}B_{\perp}/B ^b$ 10^{-4} cm^{-1}	instrument(s)
Kronos	20.3	25.4	11.4	6.0	11-14	SANS
Gemini	25.4	35.5	11.4	2.0	4.0-7.0	SANS, TAS, ANDR
Pollux	25.4	35.5	11.4	3.5	5.0-7.0	SANS, TAS, ANDR
Artemis	25.4/27.9	33.0/35.5	14.0/14.6	5.0	8.0	SANS

6. Synchronization of automated AFP NMR based ^3He spin flipping

As described earlier, one of the advantages of ^3He NSF's over conventional solid state neutron polarizing devices is the inversion of the ^3He polarization using the AFP NMR technique. Unlike the precession-coil type flipper for which control of the neutron spin state is simply controlled by turning the currents of flipping and cancellation coils off or on, control of the ^3He AFP spin flipper is more complicated. First, a National Instrument data acquisition card[67] is used to

Table 2. Magic boxes used on the BT-7 TAS beamline. l , w , and h is the overall length, width and height in cm of the box, B_0 is the field of the magic box for the ^3He polarization relaxation measurement. $|\vec{\nabla}B_{\perp}/B|^i$ is the volume-averaged field gradient determined from T_1 's measured without any stray field for a cylindrical cell typically 12 cm in diameter and 8 cm long. $|\vec{\nabla}B_{\perp}/B|^{\text{bl}}$ is the volume-averaged gradient determined from T_1 's measured with modest stray fields from the BT-7 instrument. Cowboy is a single-layer box and Flattop is a double-layer box as discussed in the text.

magic box name	l cm	w cm	h cm	field mT	$ \vec{\nabla}B_{\perp}/B ^i$ 10^{-4} cm^{-1}	$ \vec{\nabla}B_{\perp}/B ^{\text{bl}}$ 10^{-4} cm^{-1}
Cowboy	28.4	40	15	0.9	6.3	
Flattop	28.4	40	15	0.9	4.9	up to 100
Flattop	28.4	40	15	2.9	6.1	up to 30
Flattop	28.4	40	15	3.6	6.1	8.5-23

generate a frequency-swept RF signal across the resonance frequency that is also amplitude modulated by a Gaussian function[68]. In addition, we have found that the RF signal should be isolated from the AFP coil with a mechanical relay. Synchronization of the ^3He AFP spin flipper with the user experiment has not generally been done in some neutron scattering facilities that use ^3He NSF's.

We have developed a system that allows synchronization of not only AFP NMR based ^3He polarization inversion but also FID NMR measurements for optional monitoring of a T_1 of the cell. The system consists of a PYTHON program to bridge the COM port to the RS232 interface. The PYTHON program listens to the serial port of the neutron scattering instrument computer. When a text string arrives, the program checks it against an approved list of NMR commands for handling the ^3He NSF's, then forwards it over the COM connection to the IGOR Pro software[69] where all NMR commands reside. Further, it forwards back any reply message of NMR commands over the serial port to the instrument computer. The system allows independent development of the NMR software and user-friendly interface on the instrument computer to handle all possible ^3He NSF devices (as many as possible). The system allows tracking of the ^3He polarization state (hence neutron spin state), number of AFP flips, the time stamp when the ^3He polarization is inverted which might be necessary for polarization efficiency correction before data analysis.

7. Conclusions

We have provided an overview of the polarized neutron development using ^3He neutron spin filters (NSF) at the NIST Center for Neutron Research (NCNR) during the last several years. We have applied SEOP based ^3He NSF's to a wide variety of neutron scattering instruments at the NCNR. Polarized neutronic performance for each instrument class using ^3He NSF's has been improved significantly. We have demonstrated the polarized neutronic performance (transmission or intensity, and polarizing efficiency or flipping ratio) is highly predictable when the proper polarized beam calibration is done. We have shown that this polarized beam calibration with ^3He NSF's is easy, simple and straight-forward. We have shown ^3He NSF based polarizing devices developed at the NCNR are advantageous over conventional neutron polarizers, supermirror and Heusler crystals, in achieving a higher polarized flux and spin-analyzing a wide-angle divergent beam. In some instruments we employ entirely ^3He NSF's for the polarized beam setup, while for others we employ a combination of a ^3He NSF and a

supermirror. We have developed two types of magnetostatic cavities that provide a homogeneous magnetic field environment and/or shielding to the external stray field for use on different beam lines. We have developed the ^3He polarization inversion with a nearly lossless polarization feature during inversion using the adiabatic fast passage nuclear magnetic resonance technique. We have developed several spin-exchange optical pumping systems dedicated for polarized beam experiments. We have implemented a user-friendly hardware and software interface that allows easy control of neutron spins during the user experiment. Combined with polarization efficiency correction software and simple polarized beam calibration, polarized beam instrumentation at the NCNR is being established as a convenient tool. Polarized neutron experiments are routinely done on the thermal TAS, SANS, and reflectometer and will soon be established on MACS. Combined with conventional polarized beam techniques such as reflectometry, neutron spin echo, and cold triple axis spectrometry, polarized neutron measurement capabilities have been significantly enhanced at the NCNR.

Acknowledgments

We thank Jeff Anderson, Jack Fuller, Aaron Kirchhoff of the NIST glassblowing and optical shops. We acknowledge Gordon Jones for his great help in ^3He neutron spin filter development. We also acknowledge J.A. Borchers, J.W. Lynn, C.F. Majkrzak, C.L. Broholm, J.G. Barker for their scientific guidance of the polarized neutron development. The development and application of neutron spin filters has been supported during the time period of this work in part by the U.S. Dept. of Energy, Basic Energy Sciences. The work utilized facilities supported in part by the National Science Foundation under Agreement No. DMR-0944772.

References

- [1] Halpern O, Johnson MH 1939 *Phys. Rev.* bf 55 898
- [2] Maleyev SV, Baryakhtar VG, Suris RA 1963 *Sov. Phys. Solid State* **4** 2533
- [3] Blume M 1963 *Phys. Rev.* **130** 1670
- [4] Marshall W, Lowde RD 1968 *Rep. Prog. Phys.* **31** 705
- [5] Moon RM, Riste T, and Koehler WC 1969 *Phys. Rev.* **181** 920
- [6] Schärpf O and Capellmann H 1993 *Phys. Stat. Sol. A* **135** 359
- [7] Tasset F 1989 *Physica B* **156-157** 627
- [8] Brown PJ, Forsyth JB, Tasset F 1993 *Proc. R. Soc. London A* **442** 147
- [9] Abragam A 1961 *The Principles of Nuclear Magnetism* Oxford University Press, Oxford, England
- [10] Chen WC *et al.* 2011 *Journal of Physics: Conference Series* **294** 012003, and references therein
- [11] Andersen KH *et al.* 2005 *Physica B* **356** 103
- [12] Babcock E, Ioffe, A 2011 *Journal of Physics: Conference Series* **294** 012005
- [13] Jiang CY *et al.* 2013 *Physics Procedia* **42** 191
- [14] Beecham CJ *et al.* 2011 *Physica B* **406** 2429
- [15] Kira H *et al.* 2011 *Journal of Physics: Conference Series* **294** 012014
- [16] <http://www.ncnr.nist.gov/instruments/ng1refl/>
- [17] The decommissioned BT-2 thermal triple-axis spectrometer at the NCNR employed Heusler crystals as both a polarizer and analyzer.
- [18] Lee SH, Majkrzak CF 1999 *Physica B* **267-268** 341
- [19] <http://www.ncnr.nist.gov/instruments/nse/>
- [20] GE Lighting Component Sales, Bldg. 315D, 1975 Noble Rd., Cleveland, OH 44117. The largest standard GE180 tubing diameter is 16 mm; the 25 mm tubing was procured through a special glass run. Certain trade names and company products are mentioned in the text or identified in an illustration in order to adequately specify the experimental procedure and equipment used. In no case does such identification imply recommendation or endorsement by the National Institute of Standards and Technology, nor does it imply that the products are necessarily the best available for the purpose.
- [21] Chupp TE *et al* 2007 *Nucl. Instrum. Meth. A* **574** 500
- [22] Gentile TR *et al* 2005 *Physica B* **356** 96
- [23] Fu CB *et al* 2011 *Physica B* **406** 2419
- [24] Ye Q *et al* 2013 *Physics Procedia* **42** 206
- [25] 80/20 Inc., 1701 South East, Columbia City, IN 46725 USA
- [26] Optigrate, Inc., 3267 Progress Drive, Orlando, FL 32826
- [27] Volodin BL *et al* 2004 *Opt. Lett.* **29** 1891
- [28] Moser C and Steckman G 2005 *Photonics Spectra* **36 (6)** 82
- [29] Huber MG *et al* 2009 *Nucl. Instrum. Meth. A* **611** 235
- [30] Huber MG *et al* 2009 *Phys. Rev. Lett.* **102** 200401; Huber MG *et al* 2009 *Phys. Rev. Lett.* **103** 179903
- [31] Chann B, Nelson I, Walker TG 2000 *Opt. Lett.* **25** 1352
- [32] Lynn J W *et al* 2012 *J. Res. Natl. Inst. Std. Technol.* **117** 61
- [33] Chen WC *et al* 2007 *Physica B* **397** 168
- [34] Chen WC *et al* 2009 *Physica B* **404** 2663
- [35] Petoukhov AK *et al* 2006 *Nucl. Instrum. Methods. A* **560** 480
- [36] McIver JW, Erwin R, Chen WC and Gentile TR 2009 *Rev. Sci. Instrum.* **80** 063905.
- [37] Cates GD, Schaefer SR and Happer W 1988 *Phys. Rev. A* **37** 2877
- [38] Jones GL *et al* 2006 *Physica B* bf 385-386 1131
- [39] Jones GL 2000 *et al Nucl. Instrum. Meth. A* **440** 772
- [40] Majkrzak C 1991 *Hanbook of Neutron Scattering* Springer-Verlag, Berlin
- [41] Wildes AR 2006 *Neutron News* **17** 17
- [42] <http://www.ill.eu/instruments-support/instruments-groups/instruments>
- [43] Kulda J *et al* 1998 *Physica B* **241-243** 136
- [44] Lee S *et al* 2008 *Phys. Rev. B* **78** 100101(R)
- [45] Tian W *et al* 2008 *Phys. Rev. B* **78** 184429
- [46] Cabrera I *et al* 2009 *Phys. Rev. Lett.* **103** 087201
- [47] Chen Y *et al* 2008 *Phys. Rev. B* **78** 064515
- [48] Wang W *et al* 2011 *Phys. Rev. B* **84** 094504
- [49] Ratcliff W *et al* 2009 *Adv. Func. Mater.* **21** 1567
- [50] Krycka KL *et al* 2009 *Physica B* **404** 2561
- [51] Krycka KL, Chen WC, Borchers JA, Maranville BB, Watson SM 2012 *J. Appl. Cryst.* **45(3)** 546
- [52] Krycka KL *et al* 2010 *Phys. Rev. Lett.* **104** 207203

- [53] Krycka KL *et al* 2010 *J. Appl. Phys.* **107** 09B525
- [54] Krycka KL, Jackson J, Borchers JA, Shih J, Briber R, Ivkov C, Grutter C, and Dennis CL 2011 *J. Appl. Phys.* **109** 07B513
- [55] Dufour C, Fitzsimmons MR, Borchers JA, Laver M, Krycka KL, Dumesnil K, Watson SM, Chen WC, Won J, Singh S 2011 *Phys. Rev. B* **84** 064420
- [56] Ueland BG *et al* 2010 *Phys. Rev. Lett.* **104** 147204
- [57] Ramazanoglu M, Laver M, Ratcliff W, Watson SM, Chen WC, Jackson J, Kothapalli J, Seongsu L, Cheong SW, and Kiryukhin V 2011 *Phys. Rev. Lett.* **107** 207206
- [58] Laver M, Mudivarthi C, Cullen JR, Flatau AB, Chen WC, Watson SM, and Wuttig M 2010 *Phys. Rev. Lett.* **105** 027202
- [59] Michels A, Honecker D, Döbrich F, Dewhurst CD, Suzuki K, and Heinemann A 2010 *Phys. Rev. B* **85** 184417
- [60] Chen WC, Erwin R, Watson SM 2013 *Physics Procedia* **42** 163
- [61] Thampy V *et al.* 2012 *Phys. Rev. Lett.* **108**, 107002
- [62] Rodriguez-Rivera A *et al* 2008 *Meas. Sci. Technol.* **19**, 034023
- [63] Quintessence Photonics Corporation, 15632 Roxford Street, Sylmar, California 91342
- [64] Chen WC *et al.* 2003 *Physica B* **335**, 196
- [65] Chen WC, Gentile TR, O'Donovan KV, Borchers JA, Majkrzak CF 2004 *Rev. Sci. Instrum.* **75** 3256
- [66] Magnetic Shield Corporation, 740 N. Thomas Drive, Bensenville IL 60106. CO-NETIC mu-metal has a higher magnetic permeability than that of NETIC mu-metal.
- [67] USB 6251 DAQ card, National Instruments, Austin TX
- [68] McKetterick TJ *et al.* 2011 *Physica B* **406** 2436
- [69] WaveMetrics Inc. 10200 SW Nimbus, G-7 Portland, OR 97223